AD-A150 864 BONDING INFORMATION FROM AUGER SPECTROSCOPY(U) GEORGE WASHINGTON UNIV WASHINGTON D C DEPT OF CHEMISTRY D E RAMAKER NOV 84 TR-14 N00014-80-K-0852 1/1

UNCLASSIFIED F/G 7/4 NL

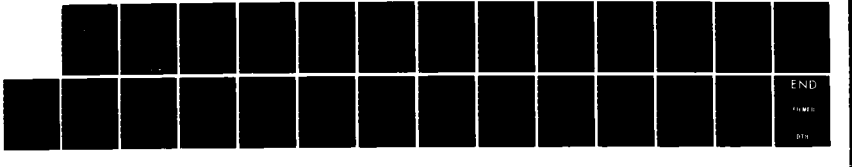

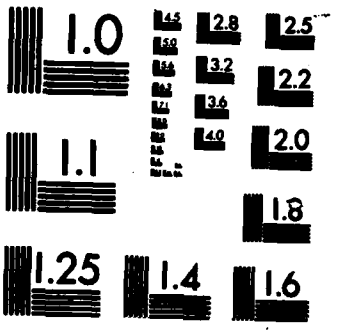

OFFICE OF NAVAL RESEARCH

N00014-80-K-0852

Task No. 056-681

Technical Report No. 14

BONDING INFORMATION FROM AUGER SPECTROSCOPY

By

David E. Ramaker

Prepared for Publication

in the

Applications of Surface Science

George Washington University
Department of Chemistry
Washington, D.C. 20052

November 1984

85 02 2. 04 C

A150 864.

SECURITY CLASSIFICATION OF THIS PAGE (When Data Entered)

REPORT DOCUMENTATION PAGE	READ INSTRUCTIONS BEFORE COMPLETING FORM
1 REPORT NUMBER: No. 14	2 GOVT ACCESSION NO: AD-A150864
3 RECIPIENT'S CATALOG NUMBER	
4 TITLE (and Subtitle): BONDING INFORMATION FROM AUGER SPECTROSCOPY	5 TYPE OF REPORT & PERIOD COVERED: Technical Report
6 PERFORMING ORG. REPORT NUMBER	
7 AUTHOR(s): David E. Ramaker	8 CONTRACT OR GRANT NUMBER(s): N00014-80-K-0852
9 PERFORMING ORGANIZATION NAME AND ADDRESS: Chemistry Department, George Washington University, Washington, D.C. 20052	10 PROGRAM ELEMENT, PROJECT, TASK AREA & WORK UNIT NUMBERS: Prog. Elem. No. 61153N, Task Area No. PP 013-08-01, Work Unit # NR056-681
11 CONTROLLING OFFICE NAME AND ADDRESS: Office of Naval Research, Dept. of Navy, 800 N. Quincy Street, Washington, D.C. 22217	12 REPORT DATE: Nov. 1984
	13 NUMBER OF PAGES: 44
14 MONITORING AGENCY NAME & ADDRESS(if different from Controlling Office)	15 SECURITY CLASS. (of this report): Unclassified
	15a DECLASSIFICATION/DOWNGRADING SCHEDULE

16 DISTRIBUTION STATEMENT (of this Report)

This document has been approved for public release and sale; its distribution is unlimited.

17 DISTRIBUTION STATEMENT (of the abstract entered in Block 20, if different from Report)

18 SUPPLEMENTARY NOTES

Submitted for publication in Applications of Surface Science.

19 KEY WORDS (Continue on reverse side if necessary and identify by block number)

Auger electron spectroscopy, screening, localization, graphite, carbides.

20 ABSTRACT (Continue on reverse side if necessary and identify by block number)

The use of Auger Spectroscopy to obtain bonding and electronic structure information is reviewed. The methods for extracting the Auger lineshape from the experimental spectrum are described; in particular the background substraction and loss deconvolution techniques are presented. A prescription is given for quantitatively interpreting the lineshape utilizing an empirically determined one-electron DOS and atomic Auger matrix elements. Final state hole-hole correlation or localization effects on the lineshape are emphasized. The carbon KVV lineshapes of graphite, diamond, and the carbides are examined. Localization

DD FORM 1 JAN 73 1473 EDITION OF 1 NOV 65 IS OBSOLETE S/N 0102-014-6601 | Unclassified SECURITY CLASSIFICATION OF THIS PAGE (When Data Entered)

Cont'd

effects in the lineshapes are correlated with ionic bonding character.

Originator Supplied Keywords include:)

See 1D14731 (Field 19)

BONDING INFORMATION FROM AUGER SPECTROSCOPY

David E. Ramaker
Chemistry Department
George Washington University
Washington, D.C. 20052

The use of Auger Spectroscopy to obtain bonding and electronic structure information is reviewed. The methods for extracting the Auger lineshape from the experimental spectrum are described; in particular the background substraction and loss deconvolution techniques are presented. A prescription is given for quantitatively interpreting the lineshape utilizing an empirically determined one-electron DOS and atomic Auger matrix elements. Final state hole-hole correlation or localization effects on the lineshape are emphasized. The carbon KVV lineshapes of graphite, diamond, and the carbides are examined. Localization effects in the lineshapes are correlated with ionic bonding character.

I. INTRODUCTION

For more than a decade now, Auger Electron Spectroscopy (AES) has been utilized as a technique for elemental identification and trace analysis at the surface of solids (1). Indeed over these years AES has become a widely available and almost indispensable technique for determining surface cleanliness, surface coverage and depth profiling. More recently, the Auger lineshape has been recognized as a source of chemical and electronic structure information. Extraction of this information from the Auger lineshape requires a thorough understanding of the factors contributing to the Auger process. This work will examine several of these factors.

To obtain chemical or electronic structure information from Auger spectroscopy requires two major efforts, first one must extract a quantitative Auger lineshape from the Auger spectrum, and second one must derive a theoretical framework for semiquantitative interpretation of that lineshape. Sec. II of this work examines current methods for extracting the lineshape. Sec. III summarizes a theoretical framework for the lineshape interpretation. Finally, Section IV reviews recent applications to extended covalent solids, in particular those involving the carbon atom in its varied allotropic and chemical forms.

The nature of this article is not to review the extensive literature on Auger spectroscopy, nor to examine in general the broad field of Auger spectroscopy. A large number of review articles on Auger spectroscopy (1 - 20) has appeared in recent years, making this unnecessary. Rather this article is directed toward explaining the semiempirical and semiquantitative methods

which have been utilized to interpret the Auger lineshapes of extended covalent systems. In particular the dramatic effects of final state hole -hole localization or correlation on the Auger lineshapes will be emphasized along with how these effects can be used to learn something about the chemical and electronic properties of the solid under study.

II. Extracting the Auger Lineshape.

The difficulty with obtaining a quantitative Auger lineshape is well known (21). It arises because the relatively small Auger signal sits on top of a large background, consisting of the back-scattered (redistributed primaries) and secondary electrons arising from the electron or photon beam which initiated the Auger decay. In addition, the Auger signal itself is distorted due to the inelastic losses which the Auger electrons suffer on their way out of the solid.

Although many slight variations have appeared, two basic techniques are currently in use for extracting the undistorted or "true" lineshape. These are summarized in Figs. 1 and 2 which illustrate the extraction of the S $L_{23}VV$ lineshape from a powdered sample of Li_2SO_4 pressed onto an In substrate (22). This case truly tests our capability to extract the lineshape because the Auger electrons around 100 - 150 eV lie in the region where the redistributed primary and secondary electrons contribute about equally to the background. Most other lineshapes with a higher Auger electron energy (e.g. the C KVV around 260 eV) are considerably easier to extract (23).

Fig. 2a shows the d N(E)/dE = N'(E) spectrum as measured

using a double pass cylindrical mirror analyzer (CMA) in the normal derivative mode. Fig. 1a shows the N(E) spectrum obtained by simple point to point integration of the measured spectrum choosing the constant zero point (N'(E)=0) to lie around E = 100 eV. Fig. 1a illustrates the background removal from the N(E) spectrum and Fig. 2a illustrates its removal from the derivative spectrum.

The removal of the background is best accomplished by fitting an analytical expression for the spectral distribution to the high and low energy wings of the Auger signal. Expressions for the secondary and redistributed primary contributions have been derived previously from theoretical analysis of the secondary cascade process in metals and the Bethe expression for electron scattering (22),

$$B(E) = A\,\frac{E}{(E+E_o)(E+\phi)^m} + B\,\frac{\ln[(E_p-E)/E_b]}{[(E_p-E)/E_b]^n} + C \qquad 1)$$

The terms primary and secondary refer to the source of the electron (i.e. primaries originate from the initial excitation beam, secondaries originate from the solid). Of course the indistinguishability of the electrons precludes this distinction;nevertheless, this terminology is often used in the literature and it will be used here to distinguish the two different spectral distribution functions utilized to describe the total backscattered or loss spectrum.

The first term in eq. 1, the secondary contribution, is essentially the Sickafus (24) expression $(E+\phi)^{-m}$ multiplied by an escape factor $E/(E+E_o)$, where ϕ and E_o are the work

function and the escape probability parameter respectively (here $E_o = .35$). In the second term, the redistributed primary function, E_p and E_b are the primary electron beam energy and the binding energy of the primary loss feature just above the Auger energy. The exponents m and n are nonlinear parameters found to range experimentally from 1.5 - 3.0 and .8 - 1.5 respectively (their theoretical values are 1.5 - 2 and 2 respectively (22)).

The linear coefficients A, B, and C are obtained from a least squares fit of eq. (1) to the high energy wing of the N(E) spectrum and some estimate of the low energy wing as pictured in Fig. 1a. The actual low energy wing can not be used since as Fig. 1b shows, the distorted (experimental) Auger lineshape tails off slowly to lower energy. In the case of the d(N(E))/dE spectrum, the analytical derivative of B(E) can be used, however in the literature, most often some polynomial expression or even graphical background substraction procedure has been used (21, 22). At higher energies, when the background function is slowly varying, a simple straight-line extrapolation of the high energy wing has been utilized and found to be quite adequate (e.g. for the C KVV lineshape reported in Fig. 9 (23)).

Removal of the distortion effects due to electron energy loss of the Auger electrons as they escape from of the solid is accomplished by deconvolution with a back scattered spectrum, L(E), with primary energy at or near the principal Auger energy as shown in Fig. 1b (22). Mathematically this can be written

$$A(E) = \int A_t(\varepsilon)\ L(E-\varepsilon)\, d\varepsilon \qquad (2)$$

where A and A_t are the "experimental" and "true" Auger lineshapes. In practice $A_t(E)$ is obtained by an iterative deconvolution procedure due to Van Cittert (25). The deconvolution also removes experimental resolution effects of the analyzer since the elastic peak of L(E) has been broadened by this same amount. The loss and elastic contribution to L(E) must be weighted by a parameter to account for the different geometrical relationships of the Auger and backscattered loss processes; i.e., the internally created Auger electrons transverse the solid escape region once, the backscattered electrons twice. In practice this is accomplished by introducing a parameter ($1 - \varepsilon$) which weights the loss contribution such that $A_t(E)$ has zero intensity at energies sufficiently below all of the features (26).

The parameter ($1 - \varepsilon$) also compensates for uncertainties in the background removal procedure (22). Figs. 1 and 2 illustrate this and some of the uncertainities which arise in $A_t(E)$. Removal of the background from N(E), as in Fig. 1, leaves in question just where the low energy wing lies. Two estimates of A(E) are illustrated in Fig. 1b. Deconvolution with the optimum values of ($1 - \varepsilon$) gives two different $A_t(E)$ curves. The optimum value of ($1 - \varepsilon$) partially compensates for the different A(E) estimates, yet some uncertainity in $A_t(E)$ still remains. Notice that the uncertainty in $A_t(E)$ increases to lower energy; this must always be recognized when quantitatively interpreting the Auger lineshape. Fig. 2a illustrates even greater problems when removing the background from the derivative mode. Because error is accumulated in the integration process, very small

$$N_{\ell_2} * N_{\ell_1}(E) = \int N_{\ell_2}(E-\epsilon) N_{\ell_1}(\epsilon)\, d\epsilon \,, \qquad 4)$$

U is the effective hole-hole Coulomb repulsion parameter, and f[ ] denotes the distortion effects caused by hole-hole localization effects. Each of these quantities are discussed in the subsections below.

III. 1 Density of States

Central to any interpretation of the Auger lineshape is a knowledge of the bulk valence band DOS. These may be obtained from theoretical calculations or from the "one-electron" spectroscopies such as x-ray emission or photoelectron spectroscopy (XES or PES). As an example, for the carbon KVV lineshape in graphite, Murday and Co-workers obtained the p DOS (both the p_σ and p_π) from angle resolved C K XES data and the s DOS from XPS data (31). Similar approaches have been utilized to obtain the DOS for BeO, Si, SiO_2, and NO_3^- (29, 30, 32, 33).

One might be led to question the utility of Auger lineshape analysis if a knowledge of the one-electron DOS is currently required before one begins the lineshape interpretation. However, AES has much greater surface sensitivity compared with XES, and the site specificity of the valence band DOS probed by AES compared with the all-sites DOS probed by PES offer additional unique advantages (1 - 28) This is particularly true for many practical systems where large inhomogenities in sample composition and complex chemical mixtures arise. Furthermore, we shall see in Sec. IV that even in simple homogenous solids, AES provides electronic structure and bonding information complementary to a

knowledge of the one-electron DOS. As the theory of Auger lineshapes further develops, it is hoped that in the future, the one-electron DOS may also be obtained from the lineshape.

III. 2 Atomic Matrix Elements

The atomic Auger matrix elements have been calculated for much of the periodic table within a one-electron Hartree-Fock-Slater approximation by McGuire (34, 35) and Walters and Bhalla (36, 37). Their results for KLL transitions at low atomic number are compared with experimental data in Fig. 3 (6). The matrix element per filled shell, $A_{c\ell\ell'}$, (i.e. per s^2, p^6, d^{10}, etc) is plotted. $A_{c\ell\ell'}$ is defined by the expressions (38)

$$A_{c\ell\ell} = \frac{(4\ell+2)(4\ell+1)}{(4\ell+2-n)(4\ell+1-n)} \times (A_{c\ell\ell})_{act.} \qquad 5)$$

$$A_{c\ell\ell'} = \frac{(4\ell+2)}{(4\ell+2-n)} * (A_{c\ell\ell})_{act.} \qquad 6)$$

where n is the number of holes in the initial ℓ shell and $(A_{c\ell\ell'})_{act.}$ is the actual Auger matrix element or experimental intensity (it is assumed the ℓ' shell in eq. (6) is filled). Since generally one is only interested in the relative $A_{c\ell\ell'}$ intensities, they have been normalized such that A_{cpp} is 100 for all Z. The matrix element per electron $P_{c\ell\ell'}$, as required in eq. (3), can be obtained from $A_{c\ell\ell'}$ by the simple relationship

$$P_{c\ell\ell'} = \frac{1}{(4\ell+2)(4\ell'+2)} A_{c\ell\ell'} \qquad 7)$$

Similar results for the $L_{23}VV$ transition with Z = 10 - 36,

and for the KL_1V and $KL_{23}V$ transitions with Z = 10 - 88 have been plotted elsewhere (6, 38). In both the KVV and $L_{23}VV$ data, the theoretical results of McGuire, and Walters and Bhalla have been scaled to the experimental results of the inert gases. Scale factors (ranging from 0.59 to 2.86) significantly different from 1 were required. These scale factors reflect the magnitude of the errors in the one-electron results. Electron correlation effects at the atomic level are clearly very important in the two valence hole final states (i.e. VV). The configuration interaction (CI) results of Chen and Crasemann (39) in Fig. 3 include electron correlation and their unscaled results agree closely with experiment. As one would expect, the $KL_{23}V$ and KL_1V one-electron results agree nicely with experiment, indicating the insignificance of correlation effects in these core-valence final states (i.e. CV) (38).

The atomic matrix element data reveal three very important points. 1) The variation of the relative Auger matrix elements with atomic number is rather small. 2) The variation that does exist is predicted remarkably well by the scaled one-electron results, indicating that the large correlation error is rather constant with Z. 3) No systematic differences between atomic gas phase, molecular phase, and solid phase experimental data exist. This is true even for the dd, pd, and pp matrix elements of the transition metals, where electron screening in the solid is expected to cause significant changes. These three points indicate that gas phase atomic data or the scaled one-electron results can be utilized for the determination of $P_{c\ell\ell'}$ in the interpretation of Auger lineshapes in the solid.

III. 3 Core Hole Screening

The core hole screening factor in eq. (3), $R_{\ell\ell'}$, accounts for the effects of core hole screening in the initial state (38, 41). Core hole screening consists of atomic radial contraction and charge transfer in response to the core hole. These effects can best be summarized by the final state (FS) rule which states that 1) the spectral distribution of each $\ell\ell'$ contribution in a CVV Auger lineshape is determined by the final DOS (i.e. in the absence of a core hole or essentially by the ground state DOS), but that 2) the relative intensity of each $\ell\ell'$ contribution is determined by the initial DOS (i.e. the DOS local to the core hole) (41). Thus the factor $R_{\ell\ell'}$ can be defined as the ratio of the integrated area of $N_\ell^* N_{\ell'}(E)$ in the presence of a core hole to that in the ground state. The FS rule also dictates that the $N_\ell^* N_{\ell'}(E)$ used in eq. (3) be that given by the final or ground state DOS. Consistent with the FS rule (42), XES and PES also reflect the ground state DOS, so that the $N_\ell(E)$ obtained empirically from these data as discussed above, are consistent with what is needed in eq. (3).

In recent work we have found that the FS rule is not always valid (38, 43). The FS rule assumes that the screening response to creation or annihilation of a core hole occurs in such a fashion that shakeoff or shakeup does not occur. Shakeoff or shakeup can be defined as the ionization or excitation of a valence electron nearly simultaneously with creation or annihilation of the core hole (i.e. shake is one aspect of the relaxation process). We have observed large amounts of shake-off in response to annihilation of the core hole by the Auger process (final state

shake-off) in the Si $L_{23}VV$ lineshape of elemental Si (38) and the S $L_{23}VV$ lineshape of Ag_2SO_4 (43). This shakeoff is exhibited by large changes in the relative $R_{\ell\ell'}$ factors. We believe that these large effects are more the exception than rule however, and we will not discuss these effects further in this work.

III. 4 Localization

The effects of final state hole-hole localization or correlation on CVV lineshapes are clearly more dramatic than the screening effects described above. In general, CVV lineshapes may range anywhere from an atomiclike lineshape (i.e. when the lineshape consist of a series of narrow lines resulting from multiplet structure) to a bandlike lineshape which reflects essentially a fold of the valence band DOS, $N_\ell(E) * N_\ell(E)$. The effective Coulomb repulsion parameter, U, is small in the bandlike case so that the the function f in eq. (3) has no effect (i.e. $f(N_\ell * N_{\ell'}(E), U \to 0) = N_\ell * N_{\ell'}(E)$). In the atomiclike case, $f(N_\ell * N_{\ell'}(E), U)$ reduces to the atomic multiplet structure so that the function f dramatically distorts the lineshape.

Cini and Sawatzky have explicitly defined the function f for CVV Auger processes in elemental solids by the expression (44),

$$f[N_\ell * N_{\ell'}(E), U] = \frac{[N_\ell * N_{\ell'}(E)]}{[1 - U\, I(E)]^2 + \pi^2 U^2 [N_\ell * N_{\ell'}(E)]^2} \qquad (8)$$

where I(E) is the Hilbert transform,

$$I(E) = \int N_\ell * N_{\ell'}(\varepsilon) / (E - \varepsilon)\, d\varepsilon. \qquad (9)$$

Two parameters essentially determine the degree of localization

of the final state holes, namely the hole-hole repulsion parameter U and the valence bandwidth V (i.e. the width of N_ℓ in eq. (8)). If U is large compared to the bandwith, the lineshape will be atomiclike ; if $V \gg U$ the lineshape will be bandlike and $f = N_\ell * N_{\ell'}(E)$. If $U \approx V$, both atomic and bandlike contributions are evident in the lineshape (44).

The results of Cini and Sawatzky were obtained by utilizing the Anderson and Hubbard many-body models (44). The equations which enter can be solved only for the initially filled band or two-hole final state. However, some work has been reported for the initially unfilled band (45), but the initial conclusions of Cini and Sawatzky do not appear to be substantially altered.

The Cini-Sawatzky results can be easily understood by considering a cluster LCAO-MO-CI approach (46). Consider a simple two-orbital system which has two holes present after the Auger process in an initially filled state (47). The holes can be described by the one-electron atomic orbitals f_a^2 and f_b^2 with binding energy ε giving the following Hamiltonian matrix:

	f_a^2	f_b^2	$\frac{1}{\sqrt{2}}(f_a f_b + f_b f_a)$
f_a^2	$2\varepsilon + U_{aa}$	0	H_{ab}
f_b^2	0	$2\varepsilon + U_{aa}$	H_{ab}
$\frac{1}{\sqrt{2}}(f_a f_b + f_b f_a)$	H_{ab}	H_{ab}	$2\varepsilon + U_{ab}$

(10)

where $U_{aa} = \langle f_a^2 \mid r_{12}^{-1} \mid f_a^2 \rangle$, $U_{ab} = \langle f_a f_b \mid r_{12}^{-1} \mid f_a f_b \rangle$, and $H_{ab} = \sqrt{2} \langle f_a \mid H \mid f_b \rangle$. Here U_{aa} and U_{ab} equals the effective one and two center hole-hole repulsions and H_{ab} equals the effective covalent interaction. Clearly if $H_{ab} < U_{aa} - U_{ab}$;

very little mixing occurs and the holes states f_a and f_b properly describe the localization of the two holes. In this instance the Auger lineshape is atomic-like and probes only the two - electron eigenstate f_a^2 (core hole site). If $H_{ab} >> U_{aa} - U_{ab}$, the mixing of the configurations is complete and the linear combinations $f_a \pm f_b$ properly describe the localization of the holes. As such, the lineshape is molecularlike (bandlike for the solid) sampling the eigenstates $1/2 * (f_a + f_b)^2$, $(f_a + f_b)(f_a - f_b)$ and $1/2 (f_a - f_b)^2$, and giving relative Auger intensities 1/4, 1/2, and 1/4 respectively. If $H_{ab} \approx U_{aa} - U_{ab}$, intermediate mixing occurs giving both contributions.

As an illustration, Fig. 4 compares the bandwidth Γ_{nd} with $U^e_{nd,nd}$ for the metals with electron configurations $d^6 s^2$ to $d^{10} s^2 p^2$ (6). For all three rows of this series the Γ and U plots cross in the region $d^8 s^2$ to $d^{10} s$. The Auger lineshapes of these "transitional" metals are given in Fig. 5 and are compared with a fold of the DOS $N * N(E)$, and in some instances the calculated atomiclike Auger lineshape (6). The lineshapes for Cu and Ag are clearly atomiclike. The lineshape for Au appears to be bandlike although shifted down in energy by 5 eV. The Ni and Pd lineshapes show atomiclike and bandlike contributions separated by 3 to 4 eV, but no multiplet structure is evident. These lineshapes illustrate the rather smooth transition from atomic to bandlike character.

In previous work, Dunlap et al (47) generalized these concepts to multielement covalent systems by providing criteria for assessing the nature of localization onto atomic, band, group, or extended band orbitals (AO, BO, GO, EBO) such as those

illustrated for $LiNO_3$ in Fig. 6. These criteria for localization can be summarized as follows:

$$\begin{aligned} &\text{AO:} && V < \Delta U_{xx} \\ &\text{BO:} && V > \Delta U_{xx}, \quad \gamma < \Delta U_{bb} \\ &\text{GO:} && \gamma > \Delta U_{bb}, \quad \Gamma < \Delta U_{gg} \\ &\text{EBO:} && \Gamma > \Delta U_{gg}. \end{aligned} \tag{11}$$

Here V is the covalent interaction between nearest neighbor carbon AO's and can be estimated from the bonding-antibonding orbital energy separation. γ is the covalent interaction between nearest neighbor BO's and can be estimated from the s and p atomic orbital energy separation. Γ is the covalent interaction between neighboring GO's; for example, the GO's are the planar arrangement of three N-O BO's about a single N atom. U_{xx}, U_{bb}, and U_{gg} are the effective Coulomb interactions between holes localized on a single AO, BO, or GO, repectively and are defined in Fig. 6.

Figure 7, utilizing a schematic one-electron DOS illustrates the covalent parameters V, γ, and Γ and the application of eq. (8) with increasingly larger values of U (48). $N(E) * N(E)$ in Fig. 7(b) is representative of the Auger line shape provided the s, s*, p, and p* bands are all filled and all localization effects are negligible, i.e., $U = \Delta U_{xx} \approx 0$. Figures (7c) - (7f) show clearly that distortion effects on each subband are reasonably independent of the other regions of the spectrum until U is sufficiently large to encompass these other regions. For U = 8.8 - 1.5 eV, no significant distortion effects occurs indicating the EBO's best describe the final state

holes. For U = 1.5 - 2.5 eV, the various $\ell\ell'$ (i.e., $\ell\ell'$ = ss, sp, etc.) subbands are distorted into narrower resonance - like features indicative of localization onto single GO's. U = 2.5 - 4 eV causes mixing of bands with bonding-antibonding character and demonstrates localization onto hybrid sp^n atomic orbitals (AO's). If the antibonding bands are empty, as in most covalent systems, localization onto the atomic orbitals will not occur because the mixing in of empty orbitals means the final state holes are being screened by other electrons and hence the effective U is decreased.

IV. Application to the C KVV Lineshapes.

The carbon atom is basic to much of chemistry, so it is not surprising that the C KVV lineshape has been reported for a wide selection of gaseous molecules and solids. The utility of AES in the gas phase, with a reduced background and narrower Auger peaks compared to the solid phase, has been clearly demonstrated (49 - 51). Figure 8 illustrates the C KVV Auger lineshape for some gas phase molecules (6). The sensitivity of AES to local hybridization (sp^3, sp^2, sp) is clearly demonstrated by the CH_4, C_2H_4, and C_2H_2 lineshapes (49). The insensitivity to substituent effects is demonstrated by the CH_4, CH_3OH, and $(CH_3)_2O$ (all sp^3) lineshapes. The normal alkanes (50) show a broadened sp^3 lineshape. The cyclic alkanes (51) show an apparent progression from the sp^2 to the sp^3 lineshape as the bond angle strain decreases. The principal peak energy in the alkanes is unchanged, inspite of the increasing size of the molecule. This suggests the final-state holes are not completely delocalized

about the molecule in these systems (i.e. the final state holes are primarily localized in some group or bond orbital). Strong localization effects have also been observed in the infinitely long alkane, polyethylene (52).

The Auger lineshapes of some of the above molecules and even smaller gas phase molecules involving C have been quantitatively interpreted using semi-empirical or ab-initio theoretical techniques. These include CO (16, 53-56), CO_2 (16, 55), C_3O_2 (57), CH_3OH (58), $Ni(CO)_4$ (56), CH_4 (58-61), C_2H_6 (51,62), C_3H_8 (51), C_2H_4 (63), and $[C(CH_3)_4]$ (64). The ab-initio techniques may include correlation effects in the configuration interaction or Green's function approaches, and reveal that even in some of these small molecules, correlation effects are clearly significant.

The Auger spectra of the various forms of C in the solid phase are also well known as shown in Fig. 9 (18, 65, 66). These spectra in the N'(E) mode are often used as "finger prints" to identify the chemical nature of impurity C atoms which are present in nearly all UHV systems (18). Many surface chemists can recognize the N'(E) "graphitic" or "carbidic" Auger lineshapes as given in Fig. 9 on sight. In spite of this familiarity, the actual Auger lineshapes, $A_{\ell\ell'}(E)$, for the C systems have not been well characterized, and even fewer attempts at quantitative interpretation have been reported. It has only been within the last few years that a few research groups have set out to really understand these C lineshapes at a fundamental level, and this work is still in progress (23).

The most thoroughly studied C Auger lineshape is that for

graphite. The first attempt at obtaining a quantitative $A_{\epsilon}(E)$ lineshape was reported by Smith and Levenson who used the procedure summarized by Fig. 2 (67). They concluded that the Auger spectrum was well characterized by a simple fold of the total DOS. An attempt at quantitatively interpreting the $A_{\epsilon}(E)$ lineshape was reported recently by Murday et al (31). They deduced the s, p_{σ}, and p_{π} DOS from XES and XPS data as described in Sec. III, assuming the electronic configuration sp^2_{σ} p_{π} per C atom. They determined the Auger lineshape from eq. (3), but assumed no hole localization effects and ignored the $R_{jj'}$ factors. They also obtained good agreement with the $A_{\epsilon}(E)$ lineshape of Smith and Levenson, however an error in the self-fold of the p DOS makes this study inconclusive.

More recently Rye et al (23) reported that the $A_{\epsilon}(E)$ lineshape of Smith and Levenson is incorrect for the very reasons discussed in Sec. III, namely the low energy wing of the Smith and Levenson lineshape has a large negative slope which has the effect of removing two much intensity from the actual Auger lineshape. The lineshape obtained by correctly forcing the low energy wing to be flat and zero is shown in Fig. 10a and is compared with the theoretical lineshape obtained from eq. (3) and U = 0. Now not even all the features are correctly reproduced by the theory.

Fig. 10b shows the much better agreement Rye et al (23) obtained by introducing values of $U_{\sigma\sigma}$ = 5 eV, $U_{\sigma\pi}$ = 1.5 eV and $U_{\pi\pi}$ = 0 eV. These U values were found to give the best fit to the experimental lineshape and reflect the magnitude of

the hole-hole repulsion in the group orbitals (i.e. the GO's consisting of 3σ or π C-C BO's in a plane). The negligible result for $U_{\pi\pi}$ reflects the zero band gap of graphite, a semimetal, although the DOS is zero at the Fermi level. The zero band gap allows for effective screening of the Auger holes by the other π band electrons so that the holes can delocalize. What is perhaps more surprising is that the $U_{\sigma\pi}$ was not reduced to zero by similar π band screening. Apparently π electrons are relatively ineffective screeners of the σ holes (23, 48).

The above results suggest that detailed lineshape interpretations of benzene and diamond would be interesting. This work is in progress so only preliminary results can be mentioned here (29). The effects of electron screening on the U values should be considerably smaller for benzene and preliminary results suggest this is the case. In diamond all valence electrons exists in the sp^3 band; i.e. no π electrons exist. The sp^3 vs $sp^2\pi$ local hybridization is clearly revealed in the lineshape of gas phase molecules as discussed above in regard to Fig. 8 (49-51). However, the much broader valence bands in the solid tend to smooth out this structure so that a comparison of the fold of the total DOS for graphite and diamond is remarkably similar (29). This suggests that the well known differences in N'(E) for graphite and diamond as shown in Fig. 9 arise primarily from different correlation effects in the σ vs the π bands, and not from differences in the one-electron DOS.

Although the difference between N'(E) for Mo_2C and SiC most certainly arises from differences in the one-electron DOS (68, 69), the more subtle differences in the transition metal carbides

(78) may arise primarily from correlation effects. Fig. 11 contains data of Smith and Levenson (71) comparing the C KVV spectra (dN/dE) for TiC, VC and Cr_3C_2. The most significant change in these spectra is the growth of a peak around 275 eV as one proceeds up the transition metal series (i.e. carbides with decreasing ionic character). The change in N'(E) in turn produces an increasing shoulder in the $A_t(E)$ lineshape. A comparison of the one-electron DOS for the carbides as calculated by Neckel et al (69) shows a slight increase in the C 2p DOS near the Fermi level and a large increase in the metal 3d DOS. The slight increase in the C_{2p} DOS could possibly be directly contributing to the growth of the 275 eV peak in N'(E). However, the increasing number of 3 d electrons could also allow for more screening of the two valence holes in the C GO's reducing the effective U, and hence creating a larger delocalized component in the Auger lineshape. Further quantitative study on these lineshapes is required to clarify these effects; this work is in progress (72).

In the oxides, the O CVV lineshape is highly localized, with just a small delocalized component appearing near the top of the lineshape (46, 6) as illustrated in Fig. 12 for Nb_2O_5 (73). In NbC and NbN this shoulder is even larger. The increase in the high energy shoulder correlates with decreasing ionicity in the Nb-anion bond. The increase in ionicity polarizes the bond orbitals toward the anion and this increases the hole hole repulsion, U_{gg}, and decreases the covalent interaction, Γ (see Fig. 6). Within the Cini-Sawatzky criterion, this causes increased localization

and hence a decreased high energy shoulder (delocalized component). Thus change in the high energy shoulder can be seen either by changing anion or changing cation, and in both cases the shoulder decreases with increasing ionicity in the bond.

A correlation can also be made between ionic bonding character and the nature of the localization. As the bond orbitals polarize both U_{bb} and U_{gg} increase, γ and Γ decrease. The increase of U_{bb} relative to γ raises the extent of BO localization (see Eq. 11). Thus increasing ionicity also changes the character or extent of localization from GO to BO. This is best summarized in Table 1, which surveys the oxygen and carbon compounds in which the Auger lineshapes have been studied and characterized. Lineshapes to the left of the Table can best be described as having BO localized character, those to the right have GO localized character.

V. Conclusions

The above discussions are generally qualitative in nature, because very few Auger lineshapes for the extended covalently bonded compounds have been quantatively interpreted in the context of localization. As mentioned above, a quantitative study of Auger lineshapes for benzene, diamond, the carbides, and other carbon compounds are currently in progress by several research groups (23, 28, 72). These studies should greatly assist current ongoing studies of more complex and applied carbon systems. Recent reports on such systems include studies of the C KVV lineshapes in K and Cs intercalated graphite (31, 74), activated carbon on metal surfaces (75-78), "diamond like" carbon (DLC)

films (79), metal ion implants in carbon polymeric substances (80), sputtered stainless steel-carbon composite layers (81), SiC single crystals and at metal interfaces fabricated for electronics use (82-84), C implanted in metals for hardening purposes (85), petroleum shales (86), organic impurities in Ar /Pd relays (18), and nitroaromatic explosives (87), to name just some of them. The uniqueness and convenience of AES to study these complex systems has been pointed out in Sec. I. A need for a clearer and more straight-forward understanding of the Auger lineshape still exists, however much progress in this regard has been made to date, and much progress is expected in the near future.

REFERENCES

1. P. H. Holloway, Adv. Electron. Electron Phys. 54, 241 (1980).
2. H. H. Madden, J. Vac. Sci. Technol. 18, 677 (1981); Surf. Sci. 126, 80 (1983).
3. F. P. Larkins, Appl. Surf. Sci. 13, 4 (1982).
4. F. Metzer, Appl. Surf. Sci. 7, 289 (1981).
5. J. C. Fuggle, "Electron Spectroscopy: Theory, Technique, and Applications:. 4, ed. C. R. Brundle and A. D. Baker (Academic Press, N.Y., 1981) p. 85
6. D. E. Ramaker, "Chemistry and Physics of Solid Surfaces IV", ed. R. Vanselow and R. Howe (Springer Verlag, Berlin, 1982), p. 19.
7. D. R. Jennison, J. Vac. Sci. Technol. 28, 548 (1982).
8. R. Weissmann and K. Muller, Surf. Sci. Reports 1S5, 251 (1981).
9. W. Moddeman and K. Wittberg, "Electron Spectroscopy: Theory, Techniques, and Applications". ed C. R. Brundle and A. D. Baker (Academic Press, NY, 1984).
10. R. R. Rye and J. E. Houston, Accounts of Chem. Res. 17, 41 (1984).
11. J. A. D. Matthew, Physica Scripta T6, 79 (1983).
12. G. G. Kleiman, Applic. Surf. Sci. 11/12, 730 (1982).
13. J. T. Grant, Applic. Surf. Sci. 13, 35 (1982).
14. H. Aksela Acta Univ. Ouluensis A 89 Phys. 15 (1980); J. Vayrynen, Acta Univ. Ouluensis, A 99 Phys. 19 (1980).
15. G. D. Stucky, R. R. Rye, D. R. Jennison, and J. A. Kelber, J. Amer. Chem. Soc. 104, 5951 (1982).
16. H. Agren, J. Chem. Phys. 75, 1267 (1981).
17. P. Weightman, Rep. Prog. Phys. 45, 753 (1982).
18. S. I. J. Ingrey, Can. J. Spec. 28, 73 (1983).
19. L. L. Levenson, Scan. Elect. Micro. IV, 1643 (1983).

20. J. C. Riviere, to be published.

21. L. A. Harris, J. Appl. Phys. 39, 1419 (1968), J. T. Grant, J. Vac. Sci. Technol. A2, 1135 (1983).

22. D. E. Ramaker, J. S. Murday, and N. H. Turner, J. Electron Spectrosc. Related Phenom. 17, 45 (1979).

23. R. R. Rye, J. E. Houston, J. W. Rogers, F. L. Hutson, and D. E. Ramaker, to be published.

24. E. W. Sickafus, Rev. Sci. Instrum. 42, 933 (1971); Phys. Rev. B16, 1436 (1977).

25. R. W. Madden and J. E. Houston, J. Appl. Phys. 47, 3071 (1976).

26. R. W. Madden and J. E. Houston, Solid State Commun. 21, 1081 (1977); J. Vac. Sci. Technol. 14, 412 (1977).

27. G. Hanke and K. Mueller, J. Vac. Sci. Technol A2, 964 (1984).

28. J. W. Rogers and M. L. Knotek, Applic. Surf. Sci. 13, 352 (1982).

29. F. L. Hutson and D. E. Ramaker, to be published.

30. D. E. Ramaker, C. T. Mei, and N. H. Turner, J. Vac. Sci. Technol. 20, 563 (1982), and to be published.

31. J. S. Murday, B. I. Dunlap, F. L. Hutson, and P. Oelhafen II, Phys. Rev. B 24, 4764 (1981).

32. D. E. Ramaker, J. S. Murday, N. H. Turner, C. Moore, M. G. Lagally, and J. E. Houston, Phys. Rev. B 19, 5375 (1979).

33. F. L. Hutson, D. E. Ramaker, B. I. Dunlap, J. D. Ganjei, and J. S. Murday, J. Chem. Phys. 76, 2181 (1982).

34. E. J. McGuire, Phys. Rev. 185, 1 (1969); A2, 273 (1970).

35. E. J. McGuire, Phys. Rev. A3, 1801 (1971).

36. D. L. Walters and C. P. Bhalla, Phys. Rev. A3, 1919 (1971); At. Data 3, 301 (1971).

37. D. L. Walters and C. P. Bhalla, Phys. Rev. A4, 2164 (1971).

38. E. J. McGuire, Research Report SC-RR-69-139, Sandia Laboratories (1969).

39. M. H. Chen and B. Crasemen, Phys. Rev. A8, 7 (1973); A16, 1495 (1977).

40. C. P. Bhalla, N.O. Folland, M. A. Hein, Phys. Rev. A8, 649 (1973).

41. D. E. Ramaker, Phys. Rev. B 25, 7341 (1982).

42. U. Von Barth and G. Grossman, Solid State Commun. 32, 645 (1979); Phys. Scr. 21, 580 (1980); Phys. Rev. B 25, 5150 (1982); G. D. Mahan, Phys. Rev. B 21, 1421 (1980).

43. N. H. Turner and D. E. Ramaker, J. Vac. Sci. Technol. A1, 1229 (1983).

44. M. Cini, Solid State Commun. 24, 605 (1976); Phys. Rev. B 17, 2788 (1978); G. A. Sawatzky, Phys. Rev. Lett. 39, 504 (1977).

45. M. Cini, Phys. Rev. B17, 483 (1979); G. Treglia, M. C. Desjonqueres, F. Ducastelle, and D. S. Spaanjaard, J. Phys. C 14, 4347 (1981).

46. D. E. Ramaker, Phys. Rev. B 21, 4688 (1980).

47. B. I. Dunlap, F. L. Hutson, D. E. Ramaker, J. Vac. Sci. Technol, 18, 556 (1981).

48. D. E. Ramaker, F. L. Hutson, R. R. Rye, J. E. Houston, and J. W. Rogers, Jr., J. Vac. Sci. Technol. A 2, 1146 (1984).

49. R. R. Rye, T. E. Madey, J. E. Houston, and P. M. Holloway, J. Chem. Phys. 69, 1504 (1978); R. R. Rye, J. E. Houston, D. R. Jennison, T. E. Madey, P. M. Holloway, Ind. Eng. Chem. Prod. Res. Dev. 18, 1 (1979).

50. R. R. Rye, D. R., Jennison and J. E. Houston, J. Chem. Phys. 73, 4867 (1980).

51. J. E. Houston and R. R. Rye, J. Chem. Phys. 74, 71 (1981).

52. J. A. Kelber and D. R. Jennison, J. Vac. Sci. Technol. 20, 848 (1982).

53. J. Muller, H. Agren, and O. Goscinski, Chem. Phys. Lett. 38, 349 (1979).

54. H. Agren and H. Siegbahn, Chem. Phys. Lett. 72, 498 (1980).

55. D. R. Jennison, J. A. Kelber, and R. R. Rye, Chem. Phys. Lett. 77, 604 (1981); J. A. Kelber, D. R. Jennison, and R. R. Rye, J. Chem. Phys. 75, 652 (1981).

56. D. R. Jennison, G. D. Stucky, R. R. Rye, and J. A. Kelber, Phys. Rev. Lett. 46, 911 (1981).

57. L. Karlson, L. O. Werme, J. Bergmark, and K. Siegbahn, J. Electron. Spectrosc. Related Phenom. 3, 181 (1974).

58. D. R. Jennison, Chem. Phys. Lett. 69, 435 (1980).

59. I. B. Ortenburger and P. S. Bagus, Phys. Rev. A11, 1501 (1975).

60. K. Faegri Jr. and R. Manne, Mol. Phys. 31, 1037 (1976).

61. O. M. Kvalheim, Chem. Phys. Lett. 86, 159 (1982).

62. D. R. Jennison, Phys. Rev. A 23, 1215 (1981).

63. D. R. Jennison, J. Vac. Sci. Technol. 17, 172 (1980).

64. D. R. Jennison, J. A. Kelber, and R. R. Rye, Phys. Rev. B 25, 1384 (1982).

65. T. W. Haas, J. T. Grant, and G. J. Dooley III, J. Appl. Phys. 43, 1853 (1972).

66. N. A. Chesters, B. J. Hopkins, A. R. Jones, and R. Nathan, J. Phys. C7, 4486 (1974).

67. N. A. Smith and L. L. Levenson, Phys. Rev. B16, 2973 (1977).

68. L. A. Hemstreet, Jr. and C. Y. Fong, Phys. Rev. B6, 1464 (1972).

69. A. Beckel, P. Rastl, R. Eibler, P. Weinberger, and K. Schwarz, J. Phys. C. 9, 579 (1976).

70. Ju. M. Shulga and G. L. Gutsev, J. Electron. Spect. Related Phenom. 34, 39 (1984).

71. N. A. Smith and L. L. Levenson, Phys. Rev. B16, 1365 (1977).

72. P. Pehrsson and D. E. Ramaker, to be published.

73. I. L. Singer and J. S. Murday, private communication.

74. B. I. Dunlap, D. E. Ramaker, and J. S. Murday, Phys. Rev. B25, 6439 (1982); J. Vac. Sci. Technol. 20, 900 (1982).

75. J. E. Houston, D. E. Peebles and D. W. Goodman, J. Vac. Sci. Technol. A1, 995 (1983).

76. L. Papagno, L. S. Caputi, F. Ciccacci, and C. Mariani, Surf. Sci. 128, L 209 (1983).

77. D. W. Goodman and J. M. White, Surf. Sci. 90, 201 (1979).

78. M. L. Bonzel and J. M. Kreba, Surf. Sci. 91, 499 (1980).

79. A. K. Green and V. Rehn, J. Vac. Sci. Technol. A1, 1877 (1983).

80. P. Pehrsson, Ph.D. Thesis, Catholic University.

81. S. Craig, G. L. Harding, and R. Payling, Surf. Sci. 124, 591 (1983).

82. R. Kaplan, to be published.

83. F. Bosso, L. Muehlhoff, M. Trenary, W. J. Choyke, and J. T. Yates, Jr. J. Vac. Sci. Technol. , (19).

84. M. V. Seller, M. Saha, W. Stanchina, I. Chaudry, and J. Bellina, these proceedings

85. I. L. Singer and J. S. Murday, J. Vac. Sci. Technol. 17, 327 (1980); I. L. Singer, C. A. Carosella, and J. R. Reed, Nucl. Instr. Methods 182/183, 923 (1981); I. L. Singer, Applic. Surf. Sci. 18, 28 (1984).

86. J. A. King and S. C. SubbaRao, these proceedings.

87. J. W. Rogers, Jr., H. C. Peebles, R. R. Rye, J. E. Houston, and J. S. Binkley, J. Vac. Sci. Technol. A2, 1018 (1984), J. Chem. Phys. 80, 4513 (1984).

88. R. R. Rye and J. E. Houston, J. Chem. Phys. 78, 4321, (1983).

TABLE I. Correlation Of Observed Character With Ionicity.

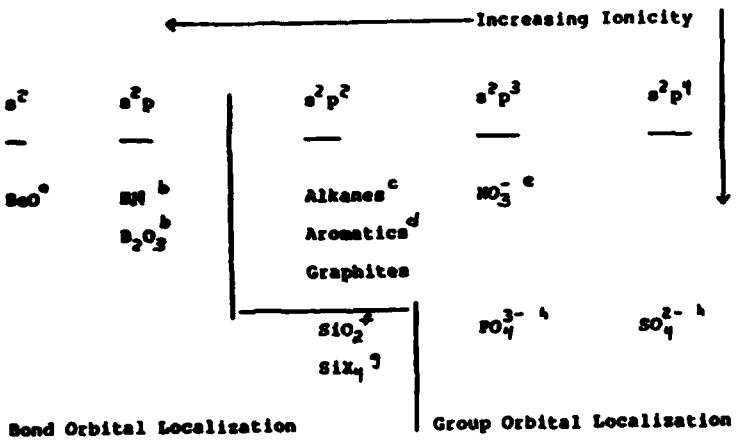

[a] Ref. 2b [b] Refs. 27 & 29 [c] Refs. 50, 51 [d] Ref. 18

[e] Ref. 33, 47 [f] Ref. 46 [g] Ref. 88 [h] Ref. 47

FIGURE CAPTIONS

Figure 1. a) The S $L_{23}VV$ Auger spectrum from Li_2SO_4 powder pressed onto an In substrate (22). The integrated signal N(E) is shown where the zero of the derivative signal shown in Fig. 2a was taken at 108 eV. The background contribution to the observed signal is indicated by the dotted line. b) The Auger lineshape A(E) obtained from N(E) - SB (E), and the elastic peak and loss features L(E) observed from a 148 eV primary beam incident on a sample of Li_2SO_4. The latter data were taken with a CMA in the normal mode and are not corrected for the analyzer transmission distortions. c) The "true" Auger signal $A_t(E)$ obtained after deconvoluting out electron-loss contributions and correcting for sample and spectrometer transmission. The solid line indicates results obtained when $(1-\mathcal{C})$ was set equal to 1.0; the dotted line when $(1-\mathcal{C})$ was set equal to 0.6 for both b) and c).

Figure 2. a) The $L_{23}VV$ Auger derivative spectrum of S from a Li_2SO_4 powder imbedded in In as measured by a double-pass CMA operating in a normal mode with a 3 eV modulation voltage (22). Two baseline estimates, determined from a non-linear least-squares fitting procedure, are indicated. b) The intergrated signal A_a and A_b obtained after removal of the baselines B_a and B_b, respectively. c) The Auger lineshape $A_t(E)$ as deduced from the data when the electron-loss features are deconvolved from A_a and A_b. The failure to achieve a flat, zero low-energy wing is caused by the way in which the background was removed.

Figure 3. Comparison of the KLL theoretical and experimental atomic Auger matrix elements $A_{\ell\ell\ell'}$ for atoms in the first two

rows of the periodic table. (16). Z is the nuclear charge, $A_{cll'}$ is the matrix element per filled shell as indicated by eq. (3). $A_{cll'}$ has been normalized for each atom such that A_{kpp} is 100. The theoretical data of McGuire (35) have been scaled by factors f_{ss} = + 0.65 and f_{sp} = 0.81, and that of Walters and Bhalla (36) by factors f_{ss} = 0.59 and f_{sp} = 0.78 to correspond to the experimental data for Ne (Z = 10). The data from Chen and Crasemann (39) are unscaled. Results of a one-electron hole calculation for Ne are indicated by the solid squares (40). The brackets indicate stated uncertainties, and the arrows indefinite estimated uncertainties in experimental data.

Figure 4. Comparison of Γ_{nd} with $U^e_{nd,nd}$ for the metals with electron configuration $d^6 s^1$ to $d^{10} s^2 p^2$(6). Metals with bandlike and atomiclike lineshapes are indicated, those between the dashed lines are "transitional".

Figure 5. Comparison of the core-(valence d)-(valence d) Auger lineshapes for the "transitional" metals as indicated in Fig. 4 with the fold of the one electron DOS, N(E) (6). The vertical bars for Cu and Ag indicate results from an atomic calculation. E_A is the core binding energy, E_A the Auger electron energy.

Figure 6. Illustration of the group, bond, and atomic orbitals (GO, BO, and AO) for $LiNO_3$. The 'effective' hole-hole repulsions, $U^e_{xx'}$, $U^e_{bb'}$, and $U^e_{gg'}$, and the corresponding interaction parameters V, Γ, or γ for NO_3^- are illustrated.

Figure 7. a) Schematic one electron DOS, N(E), and an

illustration of Γ, γ, and V as defined in the text (40). Here Γ = 2 eV, γ = 5 eV, and V = 30 eV. b) Self-fold of the one-electron DOS, N(E)*N(E) (dashed line), and the Hilbert transform I(E) (solid line). c) Comparison of N(E)*N(E) (dashed line) with A(E) (solid line) obtained from Eq. (8) with U = 1 eV. d) -f) A(E) with U = 2,3, and 10 eV, respectively.

Figure 8. The C KVV Auger lineshapes taken in the gas phase for various carbon molecules illustrating the sensitivity to sp^n hybrization (49-51).

Figure 9. The C KVV Auger spectrum, dN(E)/dE for various carbon substances in the solid phase (65, 66).

Figure 10. a) Comparison of the experimental C KVV Auger lineshape $A_C(E)$ for graphite with the theoretical lineshape computed from Eq. (3) and U = 0 and $R_{\lambda\lambda'}$ = 1. b) Same as above but with $U_{\sigma\sigma}$ = 5 eV, $U_{\sigma\pi}$ = 1.5 eV, and $U_{\pi\pi}$ = 0 (23). The individual $\mathcal{R}^{\lambda}$ (i.e. the ss, sp_σ, $p_\sigma p_\sigma$, s p_π, $p_\sigma p_\pi$, and $p_\pi p_\pi$) components are indicated by the long-short dashed lines.

Figure 11. Comparison of the Auger spectra, dN(E)/dE, for TiC, VC, and Cr_3C_2 observed by Smith and Levenson (71).

Figure 12. a) Comparison of the Nb MVV Auger spectra, dN(E)/dE, for NbC, NbN, and Nb_2O_5 as obtained by Singer and Murday (73). b) Comparison of the anion KVV Auger spectra, d N(E)/dE, for the same solids. Both the Nb and anion lineshapes reveal significant changes with ionicity.

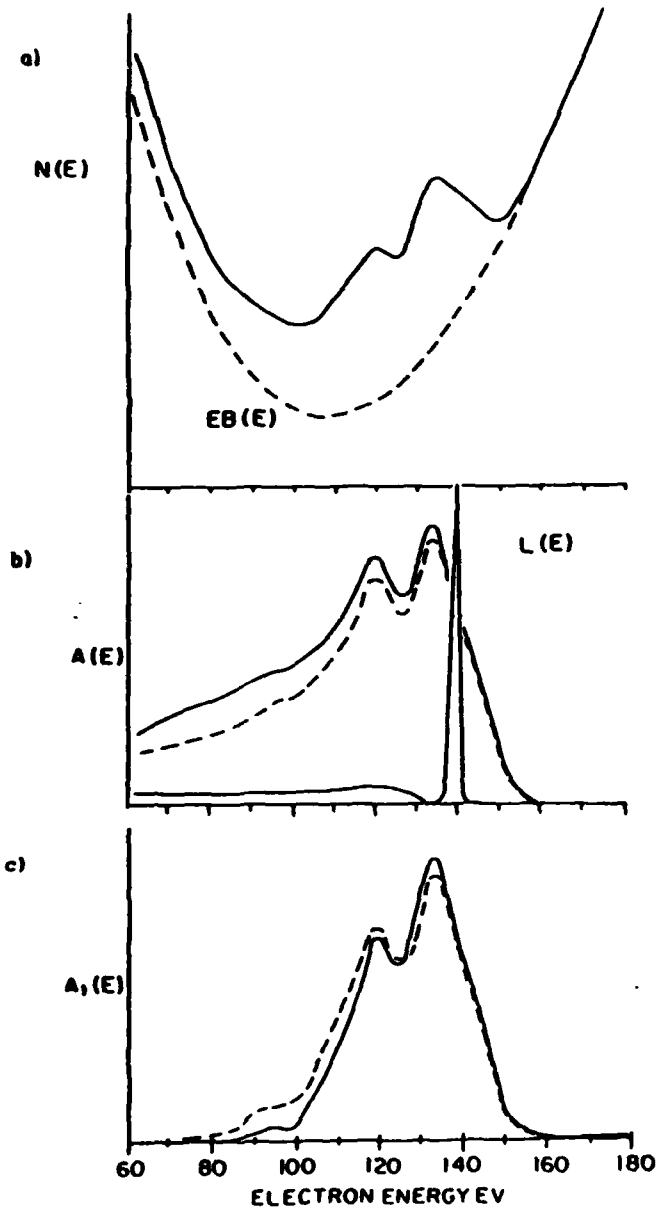
a)
N(E)
EB(E)
b)
A(E)
L(E)
c)
$A_1(E)$
60
80
100
120
140
160
180
ELECTRON ENERGY EV

1.

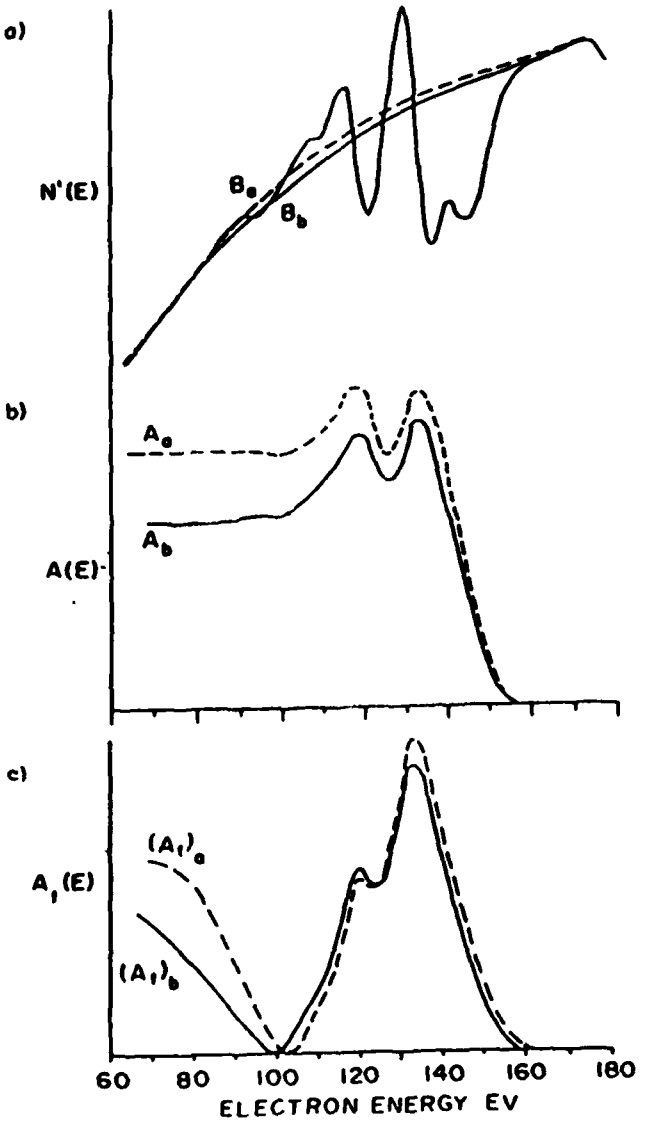
a)
N'(E)
B_a
B_b
b)
A_a
A_b
A(E)
c)
$A_1(E)$
$(A_1)_a$
$(A_1)_b$
60
80
100
120
140
160
180
ELECTRON ENERGY EV

2.

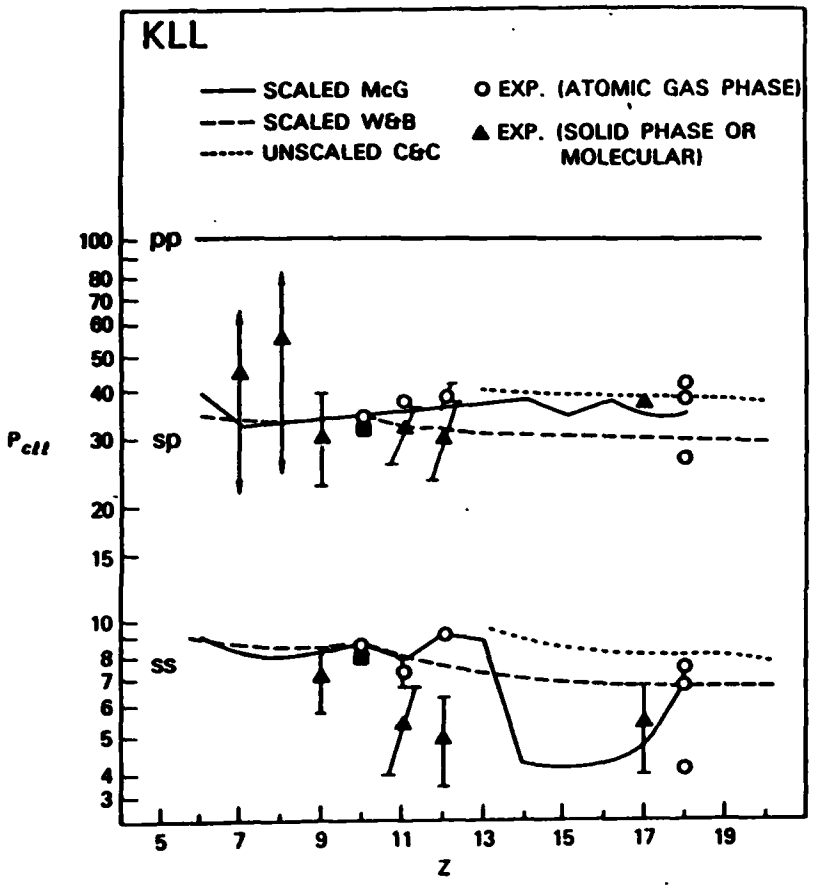
KLL
SCALED McG
SCALED W&B
UNSCALED C&C
O EXP. (ATOMIC GAS PHASE)
▲ EXP. (SOLID PHASE OR MOLECULAR)
pp
sp
ss
P_{cll}
100
80
70
60
50
40
30
20
15
10
8
7
6
5
4
3
5
7
9
11
13
15
17
19
Z

3.

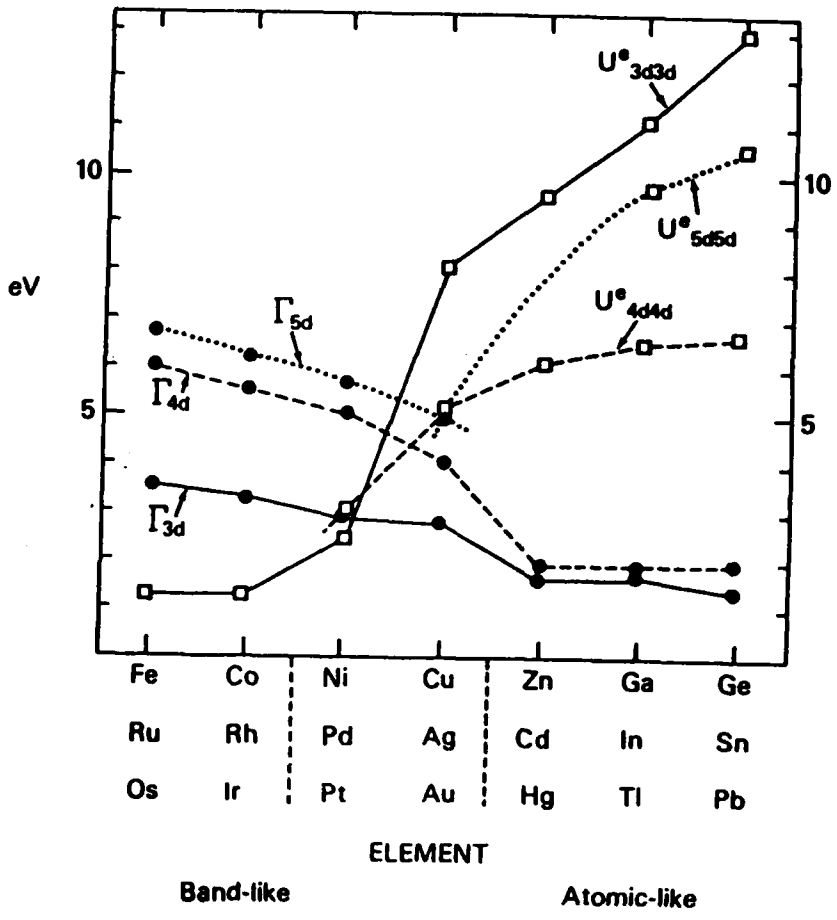
eV
10
5
U^e_{3d3d}
U^e_{5d5d}
U^e_{4d4d}
Γ_{5d}
Γ_{4d}
Γ_{3d}
Fe Co Ni Cu Zn Ga Ge
Ru Rh Pd Ag Cd In Sn
Os Ir Pt Au Hg Tl Pb
ELEMENT
Band-like
Atomic-like

4.

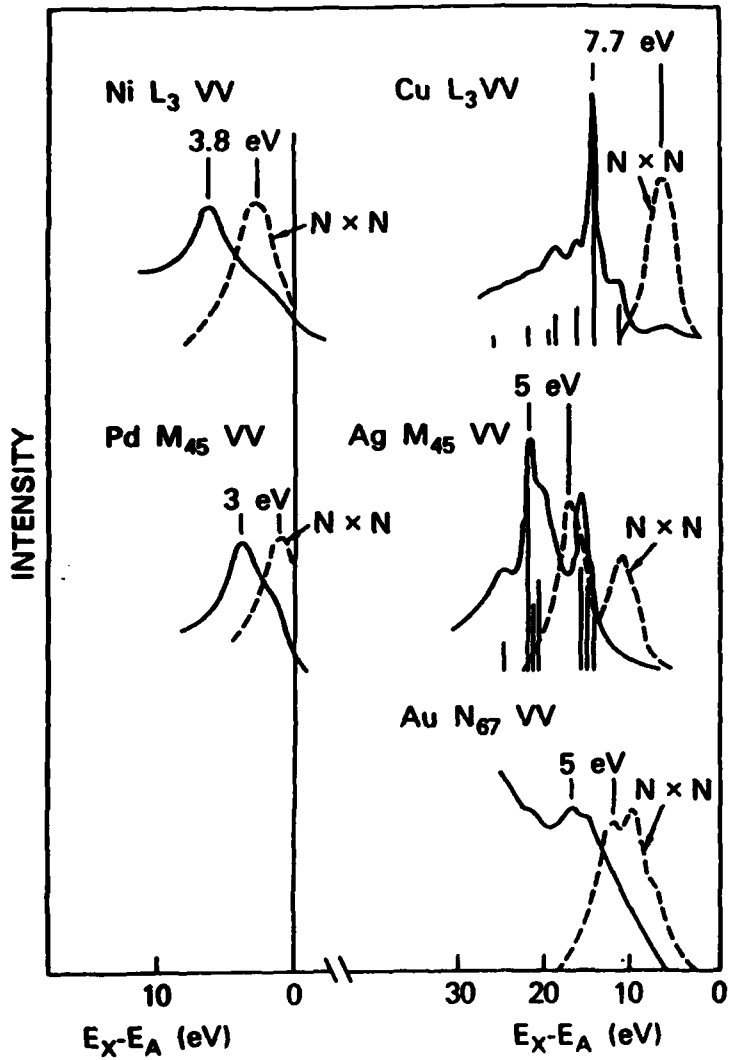
Ni L_3 VV
3.8 eV
N × N
Cu L_3VV
7.7 eV
N × N
Pd M_{45} VV
3 eV
N × N
Ag M_{45} VV
5 eV
N × N
Au N_{67} VV
5 eV
N × N
INTENSITY
10
0
30
20
10
0
E_X-E_A (eV)
E_X-E_A (eV)

5.

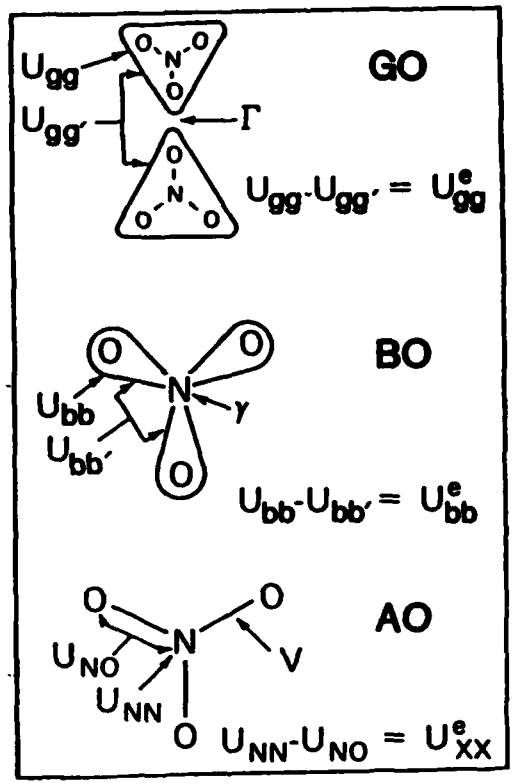
U_{gg}
$U_{gg'}$
Γ
GO
U_{gg}-$U_{gg'}$ = U^e_{gg}
U_{bb}
$U_{bb'}$
γ
BO
U_{bb}-$U_{bb'}$ = U^e_{bb}
U_{NO}
U_{NN}
V
AO
U_{NN}-U_{NO} = U^e_{XX}

6.

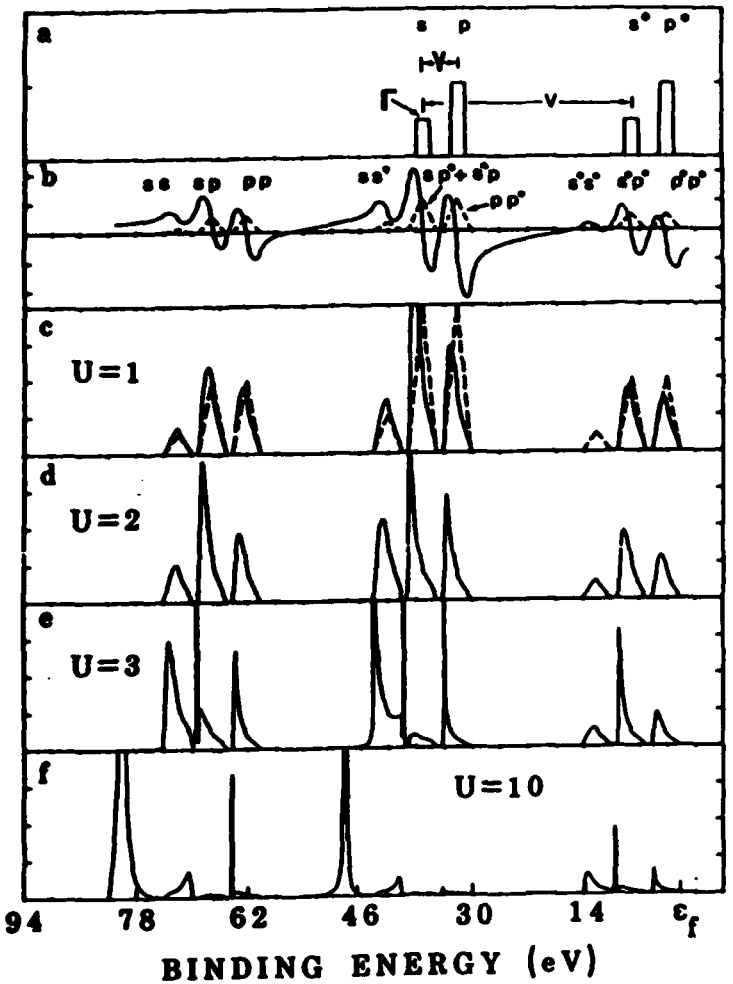
a
b
c
U=1
d
U=2
e
U=3
f
U=10
94
78
62
46
30
14
ε_f
BINDING ENERGY (eV)

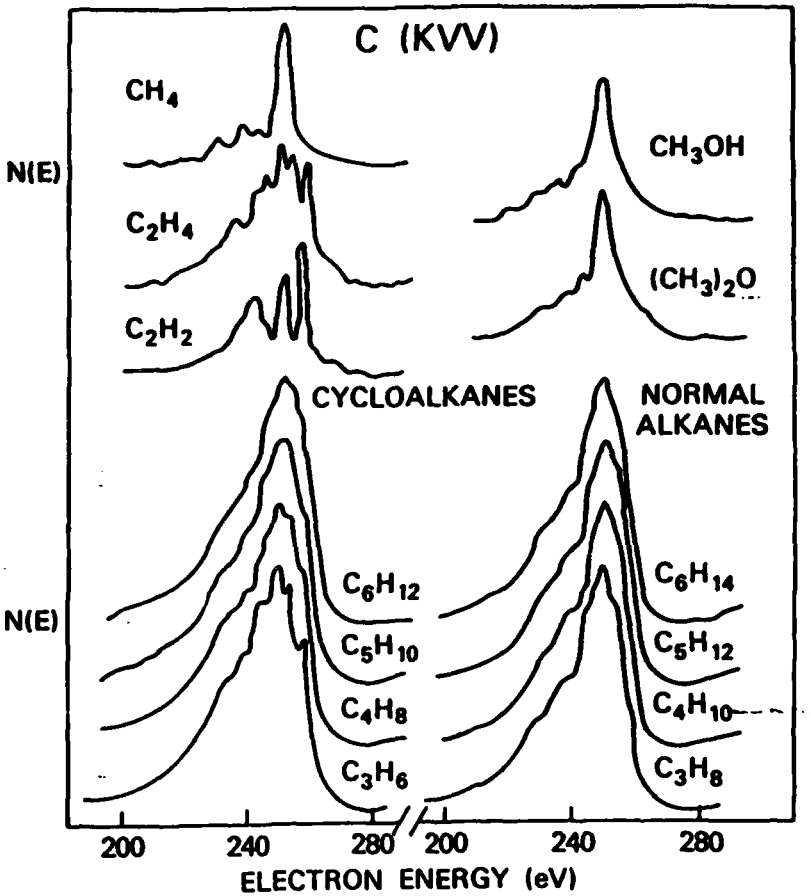
C (KVV)
CH_4
C_2H_4
C_2H_2
CH_3OH
$(CH_3)_2O$
N(E)
CYCLOALKANES
NORMAL ALKANES
C_6H_{12}
C_5H_{10}
C_4H_8
C_3H_6
C_6H_{14}
C_5H_{12}
C_4H_{10}
C_3H_8
N(E)
200
240
280
200
240
280
ELECTRON ENERGY (eV)

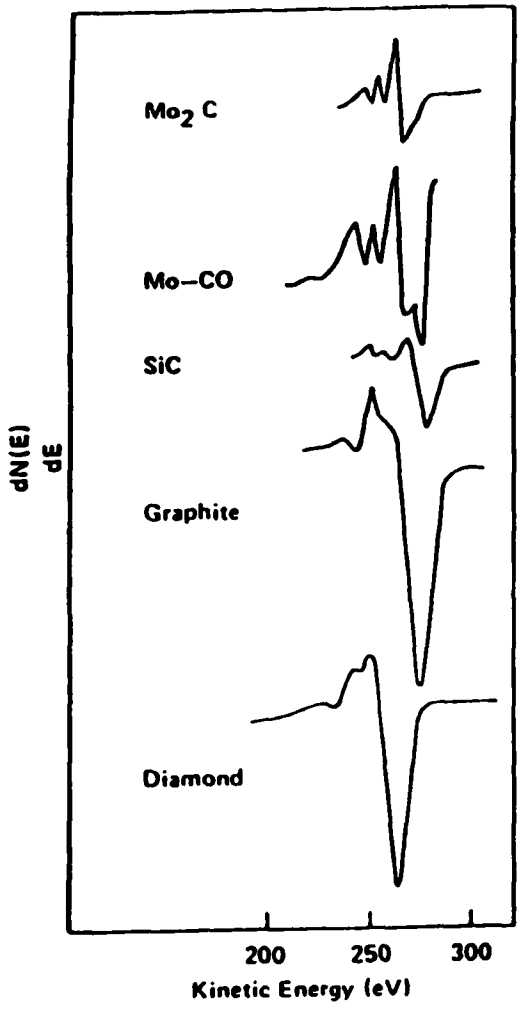
Mo2 C
Mo–CO
SiC
Graphite
Diamond
dN(E)/dE
200
250
300
Kinetic Energy (eV)

9.

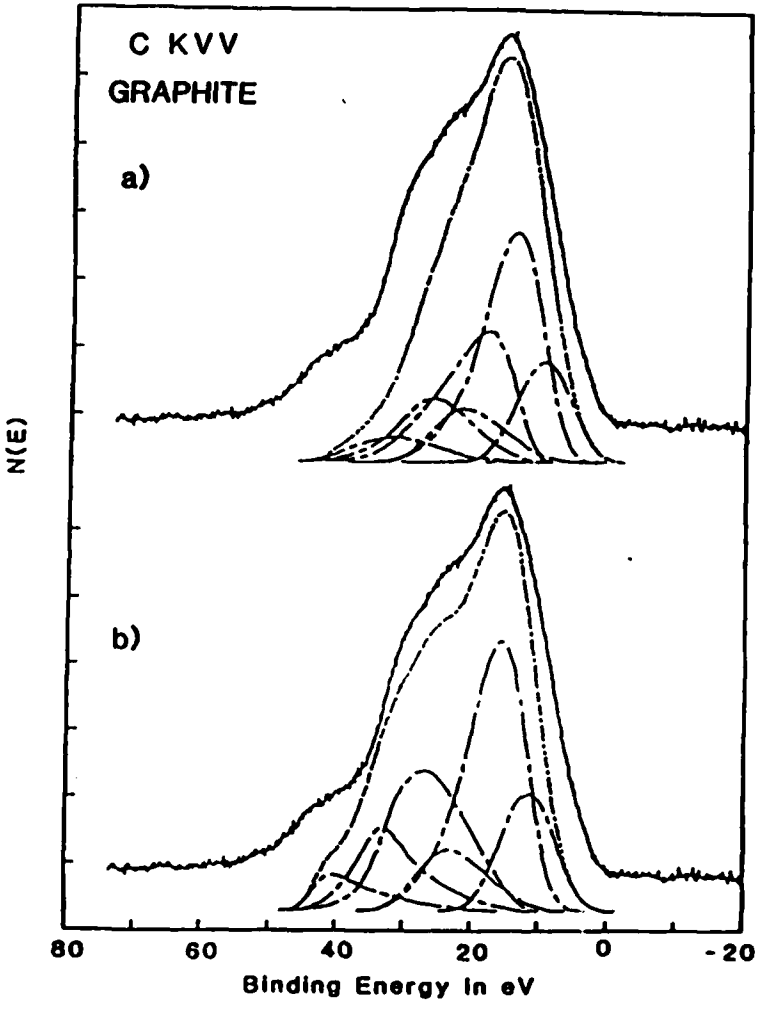
C KVV
GRAPHITE
a)
b)
N(E)
80
60
40
20
0
-20
Binding Energy in eV

10.

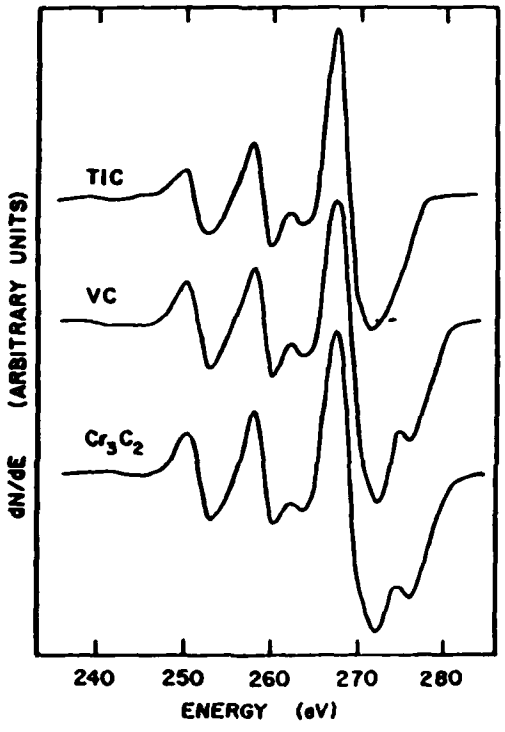
TIC
VC
Cr_3C_2
dN/dE (ARBITRARY UNITS)
240
250
260
270
280
ENERGY (eV)

11.

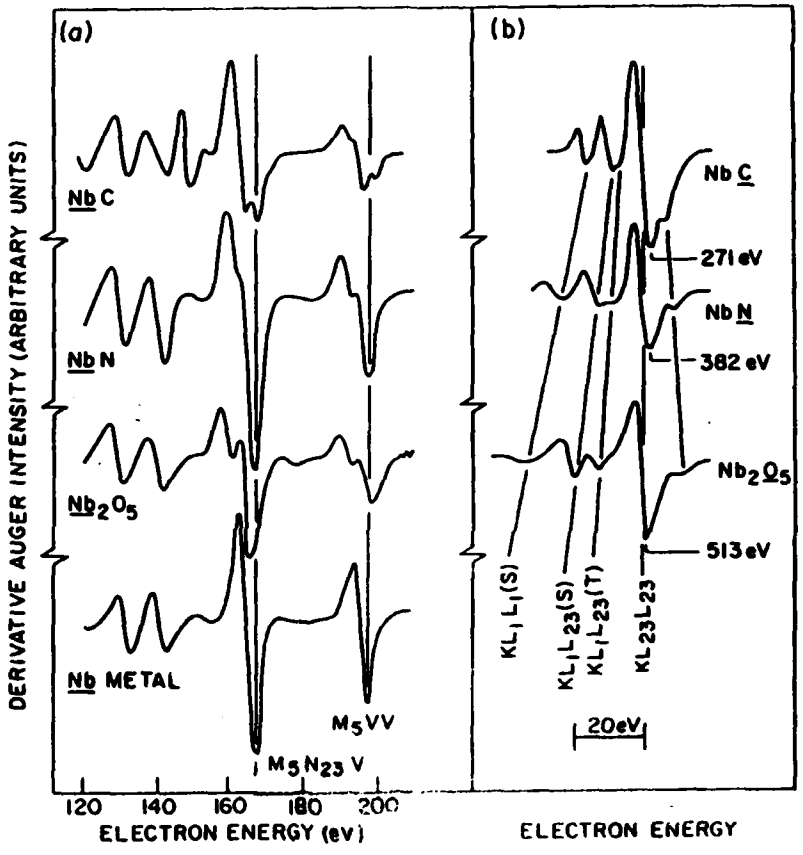
(a)
(b)
Nb C
Nb N
Nb_2O_5
Nb METAL
M_5VV
$M_5N_{23}V$
DERIVATIVE AUGER INTENSITY (ARBITRARY UNITS)
120
140
160
180
200
ELECTRON ENERGY (eV)
Nb C
271 eV
Nb N
382 eV
Nb_2O_5
513 eV
$KL_1L_1(S)$
$KL_1L_{23}(S)$
$KL_1L_{23}(T)$
$KL_{23}L_{23}$
20eV
ELECTRON ENERGY

12.

ABSTRACTS DISTRIBUTION LIST, 056/625/629

Dr. F. Carter
Code 6132
Naval Research Laboratory
Washington, D.C. 20375

Dr. Richard Colton
Code 6112
Naval Research Laboratory
Washington, D.C. 20375

Dr. Dan Pierce
National Bureau of Standards
Optical Physics Division
Washington, D.C. 20234

Dr. R. Stanley Williams
Department of Chemistry
University of California
Los Angeles, California 90024

Dr. R. P. Messmer
Materials Characterization Lab.
General Electric Company
Schenectady, New York 22217

Dr. Robert Gomer
Department of Chemistry
James Franck Institute
5640 Ellis Avenue
Chicago, Illinois 60637

Dr. Ronald Lee
R301
Naval Surface Weapons Center
White Oak
Silver Spring, Maryland 20910

Dr. Paul Schoen
Code 5570
Naval Research Laboratory
Washington, D.C. 20375

Dr. John T. Yates
Department of Chemistry
University of Pittsburgh
Pittsburgh, Pennsylvania 15260

Dr. Richard Greene
Code 5230
Naval Research Laboratory
Washington, D.C. 20375

Dr. L. Kesmodel
Department of Physics
Indiana University
Bloomington, Indiana 47403

Dr. K. C. Janda
California Institute of Technology
Division of Chemistry and Chemical Engineering
Pasadena, California 91125

Dr. E. A. Irene
Department of Chemistry
University of North Carolina
Chapel Hill, Northc Carolina 27514

Dr. Adam Heller
Bell Laboratories
Murray Hill, New Jersey 07974

Dr. Martin Fleischmann
Department of Chemistry
Southampton University
Southampton SO9 5NH
Hampshire, England

Dr. John W. Wilkins
Cornell University
Laboratory of Atomic and Solid State Physics
Ithaca, New York 14853

Dr. Richard Smardzewski
Code 6130
Naval Research Laboratory
Washington, D.C. 20375

Dr. H. Tachikawa
Chemistry Department
Jackson State University
Jackson, Mississippi 39217

OL/413/83/01
056/413-2

ABSTRACTS DISTRIBUTION LIST, 056/625/629

Dr. R. G. Wallis
Department of Physics
University of California
Irvine, California 92664

Dr. D. Ramaker
Chemistry Department
George Washington University
Washington, D.C. 20052

Dr. J. C. Hemminger
Chemistry Department
University of California
Irvine, California 92717

Dr. T. F. George
Chemistry Department
University of Rochester
Rochester, New York 14627

Dr. G. Rubloff
IBM
Thomas J. Watson Research Center
P.O. Box 218
Yorktown Heights, New York 10598

Dr. Horia Metiu
Chemistry Department
University of California
Santa Barbara, California 93106

Captain Lee Myers
AFOSR/NC
Bollig AFB
Washington, D.C. 20332

Dr. J. T. Keiser
Department of Chemistry
University of Richmond
Richmond, Virginia 23173

Dr. Roald Hoffmann
Department of Chemistry
Cornell University
Ithaca, New York 14853

Dr. J. E. Jensen
Hughes Research Laboratory
3011 Malibu Canyon Road
Malibu, California 90265

Dr. J. H. Weaver
Department of Chemical Engineering and Materials Science
University of Minnesota
Minneapolis, Minnesota 55455

Dr. R. W. Plummer
Department of Physics
University of Pennsylvania
Philadelphia, Pennsylvania 19104

Dr. E. Yeager
Department of Chemistry
Case Western Reserve University
Cleveland, Ohio 41106

Dr. N. Winograd
Department of Chemistry
Pennsylvania State University
University Park, Pennsylvania 16802

Dr. G. D. Stein
Mechanical Engineering Department
Northwestern University
Evanston, Illinois 60201

Dr. A. Steckl
Department of Electrical and Systems Engineering
Rensselaer Polytechnic Institute
Troy, NewYork 12181

Dr. G. M. Morrison
Department of Chemistry
Cornell University
Ithaca, New York 14853

Dr. P. Hansma
Physics Department
University of California
Santa Barbara, California 93106

Dr. J. Baldeschwieler
California Institute of Technology
Division of Chemistry
Pasadena, California 91125

Dr. W. Goddard
California Institute of Technology
Division of Chemistry
Pasadena, California 91125

Dr. W. Knauer
Hughes Research Laboratory
3011 Malibu Canyon Road
Malibu, California 90265

Dr. C. B. Harris
Department of Chemistry
University of California
Berkeley, California 94720

DL/413/83/01
GEN/413-2

TECHNICAL REPORT DISTRIBUTION LIST, GEN

	No. Copies
Office of Naval Research Attn: Code 413 800 N. Quincy Street Arlington, Virginia 22217	2
Dr. Bernard Douda Naval Weapons Support Center Code 5042 Crane, Indiana 47522	1
Commander, Naval Air Systems Command Attn: Code 310C (H. Rosenwasser) Washington, D.C. 20360	1
Naval Civil Engineering Laboratory Attn: Dr. R. W. Drisko Port Hueneme, California 93401	1
Defense Technical Information Center Building 5, Cameron Station Alexandria, Virginia 22314	12
DTNSRDC Attn: Dr. G. Bosmajian Applied Chemistry Division Annapolis, Maryland 21401	1
Dr. William Tolles Superintendent Chemistry Division, Code 6100 Naval Research Laboratory Washington, D.C. 20375	1
Dr. David Young Code 334 NORDA NSTL, Mississippi 39529	1
Naval Weapons Center Attn: Dr. A. B. Amster Chemistry Division China Lake, California 93555	1
Scientific Advisor Commandant of the Marine Corps Code RD-1 Washington, D.C. 20380	1
U.S. Army Research Office Attn: CRD-AA-IP P.O. Box 12211 Research Triangle Park, NC 27709	1
Mr. John Boyle Materials Branch Naval Ship Engineering Center Philadelphia, Pennsylvania 19112	1
Naval Ocean Systems Center Attn: Dr. S. Yamamoto Marine Sciences Division San Diego, California 91232	1

DL/413/83/01
056/413-2

ABSTRACTS DISTRIBUTION LIST, 056/625/629

Dr. G. A. Somorjai
Department of Chemistry
University of California
Berkeley, California 94720

Dr. J. Murday
Naval Research Laboratory
Surface Chemistry Division (6170)
455 Overlook Avenue, S.W.
Washington, D.C. 20375

Dr. J. B. Hudson
Materials Division
Rensselaer Polytechnic Institute
Troy, New York 12181

Dr. Theodore E. Madey
Surface Chemistry Section
Department of Commerce
National Bureau of Standards
Washington, D.C. 20234

Dr. J. E. Demuth
IBM Corporation
Thomas J. Watson Research Center
P.O. Box 218
Yorktown Heights, New York 10598

Dr. M. G. Lagally
Department of Metallurgical and Mining Engineering
University of Wisconsin
Madison, Wisconsin 53706

Dr. R. P. Van Duyne
Chemistry Department
Northwestern University
Evanston, Illinois 60637

Dr. J. M. White
Department of Chemistry
University of Texas
Austin, Texas 78712

Dr. D. E. Harrison
Department of Physics
Naval Postgraduate School
Monterey, California 93940

Dr. W. Kohn
Department of Physics
University of California, San Diego
La Jolla, California 92037

Dr. R. L. Park
Director, Center of Materials Research
University of Maryland
College Park, Maryland 20742

Dr. W. T. Peria
Electrical Engineering Department
University of Minnesota
Minneapolis, Minnesota 55455

Dr. Keith H. Johnson
Department of Metallurgy and Materials Science
Massachusetts Institute of Technology
Cambridge, Massachusetts 02139

Dr. S. Sibener
Department of Chemistry
James Franck Institute
5640 Ellis Avenue
Chicago, Illinois 60637

Dr. Arold Green
Quantum Surface Dynamics Branch
Code 3817
Naval Weapons Center
China Lake, California 93555

Dr. A. Wold
Department of Chemistry
Brown University
Providence, Rhode Island 02912

Dr. S. L. Bernasek
Department of Chemistry
Princeton University
Princeton, New Jersey 08544

Dr. P. Lund
Department of Chemistry
Howard University
Washington, D.C. 20059

END

FILMED

3-85

DTIC